Endo, H. Tsubota, *Earth Planet. Sci. Lett.* **23**, 136 (1974).
16. W. S. Broecker and T. H. Peng, *Tracers in the Sea* (Lamont-Doherty Geological Observatory, Columbia University, New York, 1982).
17. M. L. Delaney, L. J. Linn, P. J. Davies, *Coral Reefs* **15**, 181 (1996).
18. A. Katz, *Geochim. Cosmochim. Acta* **37**, 1563 (1973); T. Oomori, H. Kaneshima, Y. Maezato, *Mar. Chem.* **20**, 327 (1987).
19. A. J. Amiel, G. M. Friedman, D. S. Miller, *Sedimentology* **20**, 47 (1973).
20. T. S. Cross and B. W. Cross, *J. Sediment. Petrol.* **53**, 587 (1983).
21. S. de Villiers, G. T. Shen, B. K. Nelson, *Geochim. Cosmochim. Acta* **58**, 197 (1994); S. de Villiers, B. K. Nelson, A. R. Chivas, *Science* **269**, 1247 (1995); T. McConnaughey, *Geochim. Cosmochim. Acta* **53**, 151 (1989).
22. P. K. Swart, *Palaeogeogr. Palaeoclimatol. Palaeoecol.* **34**, 115 (1981).
23. The comparison is based on the following: The annual extrema of each tracer are assigned to the corresponding annual extrema of the SST record, and coral growth rate is assumed to be constant between the extrema.
24. We thank B. Parker of the Australian Institute of Marine Science for drilling the coral core and R. G. Fairbanks of the Lamont-Doherty Earth Observatory of Columbia University for helpful comments.

4 June 1996; accepted 5 September 1996

Anisotropy in the Inner Core: Could It Be Due To Low-Order Convection?

Barbara Romanowicz, Xiang-Dong Li, Joseph Durek

A recently assembled data set of inner core–sensitive free oscillation splitting measurements and body wave differential travel times provides constraints on the patterns of anisotropy in the Earth's inner core. Applying a formalism that allows departures from radial symmetry and cylindrical anisotropy results in models with *P*-wave velocity distributions whose strength and pattern are incompatible with frozen-in anisotropy, but rather suggest a simple large-scale convection regime in the inner core.

Inner core anisotropy was proposed to explain faster propagation of inner core sensitive *P* waves (*1*) on paths parallel to the Earth's rotation axis than on equatorial paths (*2*), as well as anomalous splitting of inner core–sensitive free oscillations (*3*). A model of constant cylindrical anisotropy with the fast axis parallel to the Earth's rotation axis was proposed (*4*–*10*). There has been disagreement on the strength of this anisotropy until recently (*1*, *4*, *8*, *9*), but consensus has now been reached on a strength of about 3 to 3.5%, in order to explain travel times of shallow and deep turning rays in the inner core (*10*). The debate is now focused on the physical process responsible for this anisotropy. Two classes of mechanisms have been proposed: (i) fluid inclusions in an inner core close to the melting point of its constituents (*11*), and (ii) preferential orientation of anisotropic crystals (*12*, *13*). Recent results that favor the latter interpretation include the following: (i) the expected variations in *P* wave velocity for hexagonal close packed (hcp) iron at inner core conditions match the average seismic travel time observations (*13*); (ii) recently documented existence of anisotropy in attenuation from differential PKP (BC-DF) measurements (*14*) indicates a correlation of fast velocities with high attenuation in the inner core, confirming earlier observations (*5*, *8*, *15*) and ruling out models based on fluid inclusions.

B. Romanowicz, Seismographic Station and Department of Geology and Geophysics, University of California at Berkeley, Berkeley, CA 94720, USA.
X.-D. Li and J. Durek, Seismographic Station, University of California at Berkeley, Berkeley, CA 94720, USA.

To determine whether it is convection (*12*, *16*) or freezing governed by the magnetic field (*17*) that causes the crystal alignment, we must investigate its variations in three dimensions. Most studies have only considered one-dimensional models. Departures from such models have been limited to (i) a slight tilt (~10° to 15°) of the axis of symmetry with respect to the Earth's rotation axis (*6*–*8*) and (ii) possible depth dependence of the transversely isotropic elastic tensor, resulting in a middle zone of reduced anisotropy in the inner core (*7*).

Although there is evidence for three-dimensional effects (*6*, *7*), we cannot resolve them in detail because of (i) the large number of parameters necessary to describe the most general form of anisotropy; (ii) the inadequate illumination of the inner core by body waves, due to the limited distribution of sources and receivers at the Earth's surface; and (iii) the difficulty of estimating and eliminating the effect of mantle heterogeneity. As shown in studies of mode splitting (*1*, *18*), anomalous mode splitting is dominated by zonal terms (terms that do not depend on the longitude), which are comparatively weak in the mantle (*19*, *20*). This leads us to consider, as a first approximation, models of inner core anisotropy that are three-dimensional but axisymmetric with respect to the Earth's rotation axis (or the best fitting slightly tilted axis of symmetry), thus limiting the number of free parameters.

A formalism for the inversion of normal mode splitting data for inner core anisotropy—cast in terms of general, low-degree, axisymmetric models—has been previously applied to an existing data set of inner core–sensitive modes (*21*). The resulting model, based on data for only eight modes, featured significant depth dependence but failed to provide an adequate fit to subsequent mode measurements (*22*). The occurrence of two very large, deep earthquakes in 1994 [Bolivia and Kurile Islands (*23*)] has since provided mode observations of unprecedented quality at more than 50 broadband digital stations distributed around the world. These data are being analyzed to constrain various properties of the deep Earth (*23*). We have measured the splitting of inner core–sensitive modes with the use of data from these earthquakes. Combining data for 19 such modes with differential time measurements from digital broadband stations (*24*) allows us to better constrain the deeper parts of the inner core that mode data are unable to resolve.

We applied the axisymmetric formalism (*22*) to obtain models of inner core anisotropy with various degrees of complexity. This formalism is cast in terms of spherical harmonics expansion of the anisotropic elastic tensor in the geographical coordinates (θ, ϕ) and polynomial representation as a function of radius r with further constraints that the elastic tensor must be analytical at the center of the Earth and that there are no lateral variations of Lamé parameters (*21*). The mode data are represented in terms of splitting function coefficients as defined in (*25*). The depth parameterization is quantified by ν, which is the maximum power in r of the depth dependence (ν = 0 to 4), whereas the spatial characteristics depend on n (n = 0, 2, or 4), which is related to the maximum degree of the spherical harmonics expansion. The value n = 0

Table 1. Model parameterizations for inner core anisotropy (*26*). In model #1, the transverse isotropy is constant. In models #2 and #3, it varies radially. Models #4 and #5 have an axisymmetric anistropy. X indicates that data are included in the model. Tr. times, travel times.

Data	Model number									
	1a	1b	2a	2b	3a	3b	4a	4b	5a	5b
Modes	X	X	X	X	X	X	X	X	X	X
Tr. times		X		X		X		X		X
n	0		0		0		2		4	
ν	0		2		4		4		4	

corresponds to models of transverse anisotropy parallel to the Earth's axis of rotation, with depth dependence described by ν. Thus $n = \nu = 0$ represents a model with constant transverse anisotropy (*26*).

We performed a series of inversions of the mode data, either alone or combined with a subset of our differential travel time data (*24*) for various values of ν and n (Table 1 and Fig. 1). Inversion of the modes alone, regardless of the complexity of the parameterization, yields models that do not fit the antipodal travel-time data well (Figs. 1A and 2B) because they lack sensitivity in the central half of the inner core (*10*). Joint inversion of travel times and modes produces improved variance reductions on the travel time data set (Fig. 1A and Fig. 2, C and D). Constant transverse anisotropy fails to provide a good fit to the mode data in the joint inversion (Fig. 1B). Models that allow only depth dependence of cylindrical anisotropy fare somewhat better and exhibit a minimum in strength of anisotropy midway through the inner core, as noted previously (*7*), with ~3% anisotropy in the top third of the inner core, consistent with results of previous studies.

The variance reduction of travel times and modes is further improved if we relax the constraint of radial symmetry (models #4 and #5 in Fig. 1B). These last models result in a variance reduction in the mode data set as good as with the mode data alone (Fig. 1A). In general, it is difficult to explain the observed splitting of mode 13S2 (*21*). For model #5 (Table 2 and Fig. 3), the fit to this mode as well as to other modes with large C40 components is improved over radially symmetric models (*27*). More generally, the nonradially symmetric models (#5a and #5b) allow a better fit to the C40 components (Fig. 3): the residual variance for C40 terms alone drops from 0.69 for model #3b to 0.38 for model #5b. This indicates that adding the spatial dependence ($n \neq 0$) is necessary and that the improvement of fit is not just an artifact of increasing the number of free parameters in the inversion. Moreover, for models where only depth de-

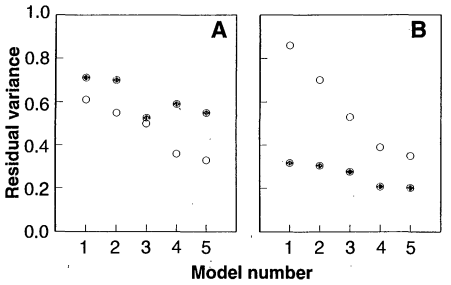

Fig. 1. Residual variances for mode-splitting data (open circles) and travel-time data (solid circles) for different model parameterizations (*26*). (**A**) Inversion with modes only; (**B**) inversion with modes and travel times. Different weighting coefficients have been tried between mode and travel-time data sets to obtain the most variance reduction in both types of data. The variance reduction from models #4b to #5b is only slight, indicating that we have reached the level of complexity resolvable with the chosen parameterization and data set.

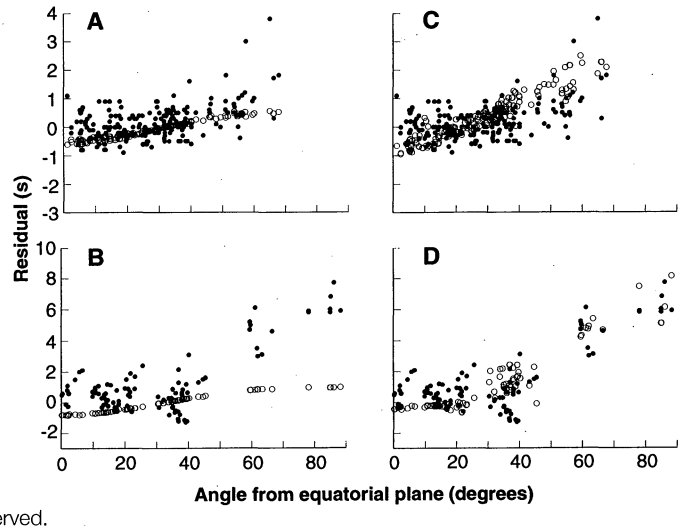

Fig. 2. Observed differential travel times (solid circles) compared to model predictions (open circles) as a function of angle of the ray path within the inner core with respect to the equatorial plane. (**A**) Predictions of model #1a for PKP(BC-DF); (**B**) same as (A) for PKP(AB-DF); (**C**) predictions of model #5b for PKP(BC-DF); (**D**) same as (C) for PKP(AB-DF). Note that at angles larger than 70°, model #5b predicts residuals of more than 2 s for (BC-DF) as well as significant scatter in (AB-DF), as observed.

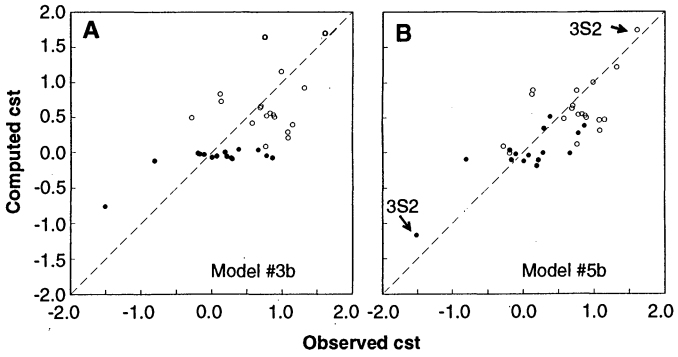

Fig. 3. Fit to mode-splitting coefficients obtained for two different models: (**A**) #3b and (**B**) #5b. Open circles are *C*20 terms. Solid circles are *C*40 terms. Units are in per mil of reference frequency. Errors in the data are estimated to be on the order of 0.5×10^{-3} to 1×10^{-3}, in general (*27*).

Table 2. Comparison of observed (Obs.) and predicted splitting coefficients (*25*) for inner core–sensitive modes used in this study. The non–radially symmetric model #5b is able to explain the *C*40 components of 13S2 and other modes with large *C*40 components better than models #3b and #1b. Units are in 10^{-6}.

Mode	*C*20				*C*40			
	Obs.	5b	3b	1b	Obs.	5b	3b	1b
3S1	−197	−11	−5	−8				
3S2	1610	1739	1699	1956	−1514	−1169	−519	−759
5S2	764	114	92	118	661	−12	43	−27
8S1	576	479	424	646				
8S5	1320	1214	92	509	−193	33	−7	−48
9S3	137	884	730	430	−814	−96	−116	−59
11S4	1079	459	299	257	276	−4	−25	−72
11S5	1086	314	214	142	−109	−24	−24	−13
13S1	−284	88	49	1618				
13S2	894	492	510	946	780	273	−41	−55
13S3	876	521	542	519	3	−120	−65	−39
16S5	1152	466	400	276	−170	−104	−17	−21
18S3	701	661	666	1097	291	342	−86	−49
18S4	831	543	565	610	214	−105	−51	−31
21S6	780	536	528	350	188	−188	9	22
22S1	756	877	1649	1626				
23S4	123	825	835	1252	866	378	−69	−53
23S5	690	622	646	761	72	−41	−46	−31
27S2	989	998	1160	1384	380	506	45	−58

pendence of cylindrical anisotropy is allowed (#1ab and #3ab), the predicted travel times cluster tightly along a single curve, whereas model #5b predicts a scatter of ~2 s at angles from the equatorial plane larger than 60°, as observed (Fig. 2, B and D).

Relaxing the constraint of radial symmetry results in an elongation, in the direction of the rotation axis, of the central zone of higher P wave velocities parallel to the rotation axis (Fig. 4). These velocities are also strong near the surface in the equatorial regions but not as strong at mid-latitudes (*29*). This latter result is in agreement with observations of travel times and amplitudes of PKP(BC) and PKP(DF) by Souriau and Romanowicz (*14*), which led them to infer that the angle [Θ] of ray paths with respect to the axis of rotation may not be the appropriate parameter to describe inner core anisotropy at higher latitudes. The variability between the models illustrates the range of possible solutions that we can obtain with the available data sets and parameterization. They have in common two zones of faster axis-parallel P wave velocities: the first one equatorial and shallow; the second, a zone concentrated around the axis of rotation with variable intensity as a function of depth, depending on the model. All models are characterized by reduced anisotropy between those two strong zones. We note that the data seem to favor a symmetry axis slightly tilted (~10°) from the Earth's rotation axis (6–8), but this is not the dominant effect in explaining the variance in the entire data set (Fig. 5). The main effect in reducing the total variance (travel times and modes) is due to relaxing the radial symmetry and cylindrical anisotropy constraint. The models obtained with the best axis of symmetry do not differ significantly from those already presented.

The patterns found (Fig. 4) are not compatible with frozen-in anisotropy related to

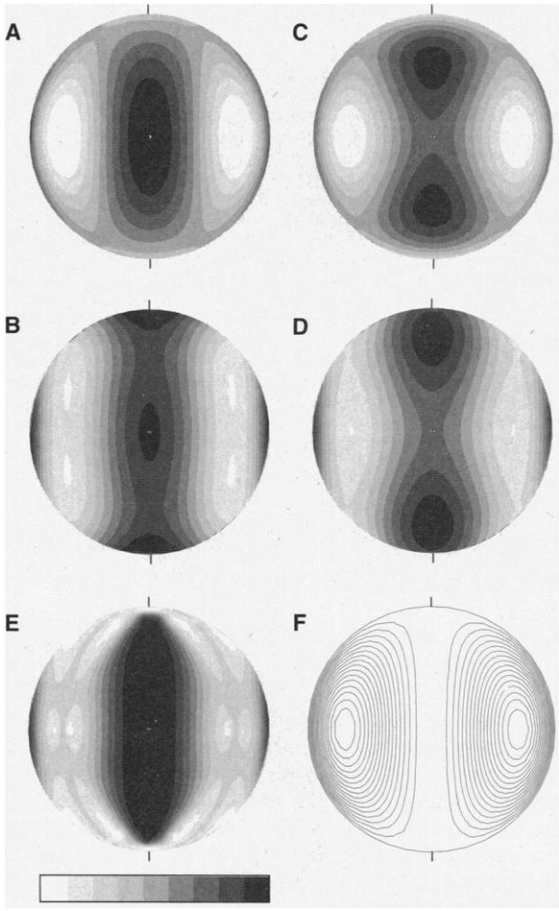

Fig. 4 (left). Cross sections of the inner core in a plane containing the rotation axis. Because of the axial symmetry of the models considered, all such planes are equivalent. The scale bar shows the residual P wave velocity in percent for (**A**) to (**E**). The scale ranges from 0 to 4% (light to dark shading) for (A) to (D) and −1 to 3% for (E). [(A) to (D)] Variations with depth and position of the velocity of P waves traveling parallel to the Earth's rotation axis, with respect to the reference P wave velocity (*28*). For radially symmetric models, the patterns would be concentric circles. Models are #4b [(A) to (B)] and #5b [(C) to (D)] where (A) and (C) are obtained with the use of the complete 19-mode data set and (B) and (D), the same data set minus three modes for which the splitting coefficients are poorly constrained (9S3, 13S1, and 5S2). (E) Predictions for a synthetic model in which we assume a mode 1 convection pattern in an inner core made of anisotropic hcp-iron crystals (*13*). (**F**) Pattern of flow lines for mode 1 convection. In the calculation, the iron crystals are assumed to align their c-axis along these streamlines. We weigh the contribution of each streamline to anisotropy by considering its position within the flow, the external parts giving the strongest alignment.

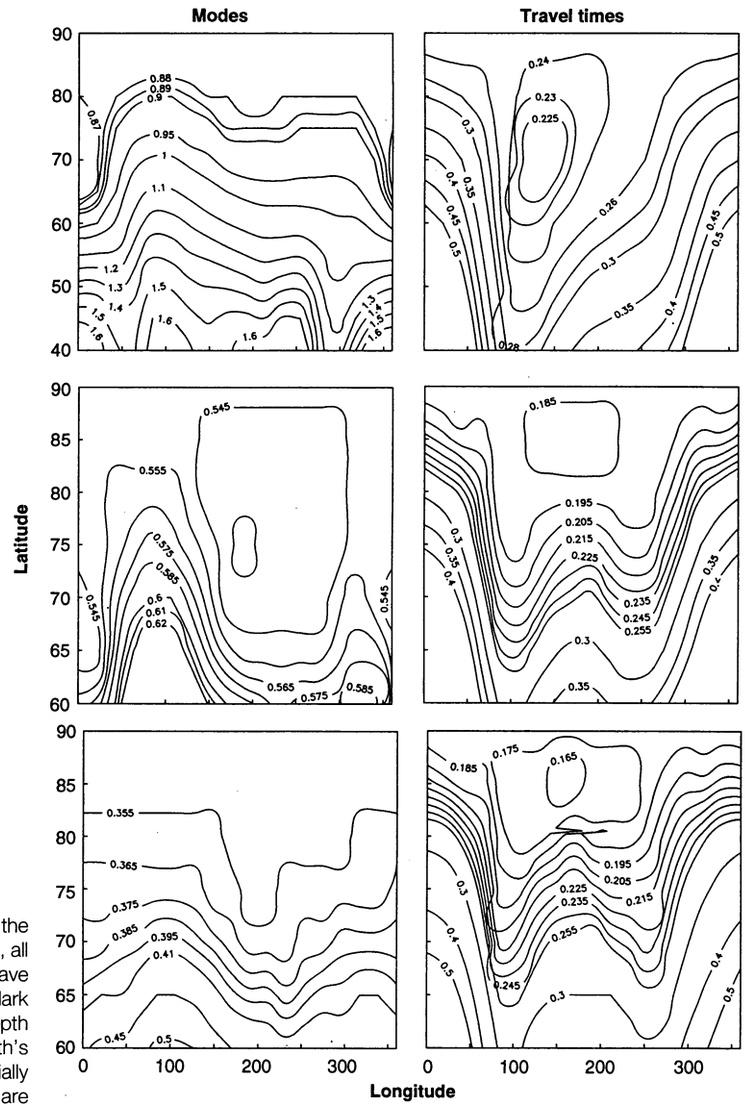

Fig. 5 (right). Contour plots showing residual variance for mode data (left) and travel time data (right) for different models, as a function of position of the symmetry axis in latitude and longitude. From top to bottom: models #1b, #3b, and #5b. For each model, the minimum is less marked in the mode data than in the travel time data, and in the latter, it shifts from a location at 70°N, 130°E (model #1b) to a location at 85°N, 170°E (model #5b).

inner core growth, which should preserve radial symmetry. They are reminiscent of what one might expect to observe if large-scale low-order convection were the dominant cause of anisotropy in the inner core (Fig. 4D). This model is oversimplified and is only shown for qualitative comparison. Note, however, that the range of predicted velocities is in good agreement with that obtained by inversion. In a convecting inner core, anisotropic effects of crystal alignment are expected to dominate over lateral heterogeneity due to density anomalies (*12*, *17*).

Mode 1 convection (Fig. 4, D and E) is not necessarily the dominant mode of convection in the inner core. The longitudinal averaging inherent in our modeling, the limited parameterization, errors in the data due to unmodeled mantle effects, and possible lateral heterogeneity in the inner core prevent us from further characterization of these patterns. However, since anisotropy extends to the center of the inner core (*10*), the likelihood of low-order convection is supported by numerical computations (*17*), which indicate that high Rayleigh number chaotic solutions would tend to concentrate effects detectable by means of anisotropy at shallow depths in the inner core. A physical explanation for why a low-order convection pattern in the inner core should align with the Earth's rotation axis remains to be found (*30*).

REFERENCES AND NOTES

1. J. H. Woodhouse, D. Giardini, X. D. Li, *Geophys. Res. Lett.* **13**, 1549 (1986); A. Morelli, A. M. Dziewonski, J. H. Woodhouse, *ibid.*, p. 1545. There are several branches of core penetrating *P* waves. PKP(DF) goes through the inner core, whereas PKP(BC) and PKP(AB) remain in the liquid outer core, assumed to be homogeneous. BC and AB are observed at distances for which DF samples the outer third and inner two thirds of the inner core, respectively.
2. G. Poupinet, R. Pillet, A. Souriau, *Nature* **305**, 204 (1983).
3. G. Masters and F. Gilbert, *Geophys. Res. Lett.* **8**, 569 (1981). Aspherical structure and anisotropy break the azimuthal degeneracy of free oscillations, leading to separation of a mode of angular order *l* into $(2l + 1)$ singlets.
4. P. M. Shearer, K. M. Toy, J. A. Orcutt, *Nature* **333**, 228 (1988).
5. X. Song and D.V. Helmberger, *Geophys. Res. Lett.* **20**, 2591 (1993).
6. P. M. Shearer, *J. Geophys. Res.* **99**, 19647 (1994).
7. W. Su and A. M. Dziewonski, *ibid.* **100**, 9831 (1994).
8. K. C. Creager, *Nature* **356**, 309 (1992).
9. J. Tromp, *ibid.* **366**, 678 (1993).
10. L. Vinnik, B. Romanowicz, L. Breger, *Geophys. Res. Lett.* **21**, 1671 (1994); X. D. Song, *J. Geophys. Res.* **101**, 16089 (1996).
11. D. J. Doornbos, *Geophys. J. Ry. Astron. Soc.* **38**, 397 (1974); D. R. Fearn, D. E. Loper, P. H. Roberts, *Nature* **292**, 232 (1981).
12. R. Jeanloz and H. R. Wenk, *Geophys. Res. Lett.* **15**, 72 (1988).
13. L. Stixrude and R. E. Cohen, *Science* **267**, 1972 (1995).
14. A. Souriau and B. Romanowicz, *Geophys. Res. Lett.* **23**, 1 (1996); *Phys. Earth. Planet. Inter.*, in press.
15. V. Cormier, *Eos* **75**, 67 (1994).
16. P. Weber and P. Machetel, *Geophys. Res. Lett.* **19**, 2107 (1992).
17. S. Karato, *Science* **262**, 1708 (1993).
18. M. Ritzwoller, G. Masters, F. Gilbert, *J. Geophys. Res.* **91**, 10203 (1986).
19. W. J. Su, R. L. Woodward, A. M. Dziewonski, *ibid.* **99**, 6945 (1994); S. Johnson, P. Shearer, G. Masters, *Eos Fall Suppl.* **75**, 475 (1994).
20. X. D. Li and B. Romanowicz, *J. Geophys. Res.* **101**, 22245 (1996).
21. X. D. Li, thesis, Harvard University (1990); ———, D. Giardini, J. H. Woodhouse, *J. Geophys. Res.* **96**, 551 (1991).
22. R. Widmer, G. Masters, F. Gilbert, *Geophys. J. Int.* **111**, 559 (1992).
23. Bolivia: 9 June 1994, depth = 647 km, moment magnitude (*Mw*) = 8.2; Kurile Islands: 10 October 1994, depth = 68 km, *Mw* = 8.3; J. Tromp and E. Zanzerkia, *Geophys. Res. Lett.* **22**, 2297 (1995); J. S. Resovsky and M. Ritzwoller, *ibid.*, p. 2301; J. Tromp, *Geol. Soc. Am. Today* **5**, 137 (1995).
24. The travel time data set comprises representative subsets of antipodal PKP(AB)-PKP(DF) data from (*10*) and of PKP(BC)-PKP(DF) data from (*14*). The mode data set consists of splitting coefficients *C*00, *C*20, and *C*40, as defined in equation 11 of (*25*), for 19 inner core–sensitive modes, measured using Bolivia and Kurile data only (*23*), and corrected for rotation, ellipticity as well as mantle effects, using (*20*). These coefficients are combined in a spherical harmonic expansion to define the splitting function, and represent integrated effects on the modes of structure from the Earth's center to the surface. Units are in ‰ of degenerate frequency of each mode. The modes considered are given in Table 2. We compared corrections for mantle structure with the use of different mantle models and found that changing the model has no significant effects on our results. Uncertainties on mantle corrections for zonal terms are on the order of 0.1‰. An *S* to *P* wave velocity conversion factor of 0.5 was used in the mantle correction computations. This choice has little effect on the inner core models obtained.
25. D. Giardini, X. D. Li, J. H. Woodhouse, *Nature* **325**, 405 (1987); *J. Geophys. Res.* **93**, 13716 (1988).
26. Models are numbered as follows: #1: $v = 0$, $n = 0$ (constant cylindrical anisotropy with axis parallel to the Earth's rotation axis, 5 parameters); #2: $v = 2$, $n = 0$; #3: $v = 4$, $n = 0$ (cylindrical anisotropy as before, with depth variation allowed in powers of r, up to r^v; 10 and 15 parameters, respectively); #4, $v = 4$, $n = 2$; (35 parameters); #5, $v = 4$, $n = 4$ (both spatial and depth variations are allowed, and the anisotropy need not be cylindrical; the number of free parameters in this case is 44).
27. The determination of the splitting coefficients is a highly nonlinear process. For some inner core–sensitive modes (13S2 and 3S2 in particular), and with the current data set, the solution space exhibits several minima, with significantly different values of the *C*20 and *C*40 terms (for example, Megnin and Romanowicz, *Eos Fall Suppl.* **76**, 46 (1995). We have verified that our solutions remain stable when we remove one or both of these modes. This is particularly important for 3S2, whose splitting dominates the mode data set (Fig. 3).
28. A. M. Dziewonski and D. L. Anderson, *Phys. Earth. Planet. Inter.* **25**, 297 (1981).
29. Previous studies have documented that the top 100 km of the inner core has little anisotropy [(*6*) and X. Song and D. Helmberger, *J. Geophys. Res.* **100**, 9805 (1995)]. Our limited parameterization with depth does not allow us to resolve this level of detail. Future studies should consider depth parameterizations in terms of layers or other local basis functions, but the price to pay will be the loss of the elegance of the formalism.

30. We thank X. Song for making his data available to us and P. Olson for helping us with the computations of streamlines for mode 1 convection, as well as two anonymous reviewers whose comments helped improve the manuscript. This research was partially supported by NSF grant EAR9417862. It is Seismographic Station contribution #9609.

6 May 1996; accepted 8 October 1996

Three-Dimensional Imaging of Single Molecules Solvated in Pores of Poly(acrylamide) Gels

Robert M. Dickson, D. J. Norris, Yih-Ling Tzeng, W. E. Moerner*

Individual fluorescent molecules and individual singly labeled proteins were observed in the water-filled pores of poly(acrylamide) gels by far-field microscopy. Brownian motion was markedly reduced by the gel framework, thus enabling extended study of single fluorophores in aqueous environments. A highly axially dependent laser field was used both to excite the fluorophores and to image the molecules in three dimensions. Single molecules were followed as they moved within and through the porous gel structure. In contrast to dry polymeric hosts, these water-based gels may form a useful medium for single-molecule studies of biological systems in vitro.

Since the first reports of optical detection of single small molecules (*1*–*3*), an important goal has been to address chemical and biological problems with the unique local environmental sensitivity that single molecules provide. One promising technique is the observation of single-fluorophore emission in flowing streams (*4*, *5*) or the use of confocal microscopy (*6*) to detect molecules directly in solution. These techniques have demonstrated their powerful analytical utility for identification of fluorophore-labeled biomolecules; for example, the detection of individual DNA strands both in solutions (*7*) and during

R. M. Dickson, D. J. Norris, W. E. Moerner, Department of Chemistry and Biochemistry, Mail Code 0340, University of California, San Diego, 9500 Gilman Drive, La Jolla, CA 92093–0340, USA.
Y.-L. Tzeng, Scripps Research Institute, 10666 North Torrey Pines Road, La Jolla, CA 92037, USA.

*To whom correspondence should be addressed.